Modelling of glass matrix composites by the Coupled Criterion and the Matched Asymptotic Approach. The effect of residual stresses and volume fraction

S. Jiménez-Alfaro, D. Leguillon

Modelling of glass matrix composites by the Coupled Criterion and the Matched Asymptotic Approach. The effect of residual stresses and volume fraction.

S. Jiménez-Alfaro[a,*], D.Leguillon[a]

[a]*Institut Jean Le Rond d'Alembert, Sorbonne Université – CNRS UMR 7190, 4 place Jussieu, 75000 Paris, France*

Abstract

The fracture toughness of glass can be improved by including ceramic reinforcing platelets. Among others, Al_2O_3 platelets are proposed as an environmentally friendly and low-cost solution. One of the critical points in the design of this composite is the generation of residual stresses after cooling in manufacture, due to the thermal expansion mismatch between the two materials. In this paper, the effect of these residual stresses and the role of the volume fraction are studied, following a methodology based on the Coupled Criterion together with the Matched Asymptotic Expansion. The model is validated through a comparison with experimental results found in the literature.

Keywords: Finite Fracture Mechanics, Coupled Criterion, Micro-scale, Fracture toughness, Residual stresses

1. Introduction

Ceramic platelets are used as a reinforcing constituent in glass matrices to improve mechanical properties such as fracture toughness [1]. One example is the borosilicate glass Al_2O_3 platelet composite, which can be really interesting for industrial applications due to its low production cost and environmental safety [2]. This kind of composite can be used in glass-to-metal seals [3], which

*Corresponding author. Tel.: +34 627241123
Email address: sara.jimenez_alfaro@sorbonne-universite.fr (S. Jiménez-Alfaro)

are widely applied in electrical penetration assemblies [4], solid oxide fuel cells [5], and implantable medical devices [6]. Adding Al_2O_3 platelets increases the fracture properties of glass, that are not enough to overcome the extreme environments that sometimes are found in the service conditions [7].

Borosilicate glass Al_2O_3 platelet composite was initially introduced by Boccaccini et al. [8]. In their study, they performed a material characterization using scanning electron microscopy (SEM). Two important aspects of the fracture behaviour were investigated: the fracture surface of the composite using reflected light microscopy, and the increase in fracture toughness of the glass when alumina is added, assessed through the singled edge notched beam (SENB) technique. As later demonstrated [9], both are correlated through the fracture surface roughness. Furthermore, new experimental measurements of the fracture toughness were conducted in [1], considering the chevron notched specimen technique. Another related study worth mentioning is [10], which focused on enhancing the fracture toughness through cold-pressing, as opposed to the original hot-pressing method introduced in [8].

One of the most important characteristics of this composite is the thermal expansion mismatch between alumina and glass [11]. The thermal coefficient in alumina is higher than the one in glass, and consequently, compressive residual stresses will appear in the matrix after cooling, as well as tensile residual stresses in the platelet [12]. The effect of this thermal mismatch have been studied experimentally and numerically. In 1999, Todd et al. [11] measured residual stresses and their toughening effect in experiments using fluorescence microscopy to relate the change in the luminiscence spectrum of alumina to stresses. They also justified the consideration of isotropic thermal properties in the platelet, since results do not differ from the anisotropic measurements. The results were compared to some theoretical models [13] and [14], based on the aspect ratio of the platelet. Then, in 2001 Cannillo et al. [12] performed numerical simulations using the finite element method (FEM) to quantify residual stresses. A special tool was used to map an image of the material microstructure for the calculation. Notably, this same tool was also applied in 2003 by Cannillo et al. [15] to

investigate how cracks are propagated in this kind of materials.

Although there exits a substantial body of literature on reinforcing glass with alumina platelets, only a limited number of studies have investigated the fracture toughness through numerical analyses. The first characterization was conducted by Cannillo et al. [16] in 2001. Subsequently, in 2022, a new methodology to design and study platelets composite was introduced in [17]. This approach is based on the application of the Coupled Criterion (CC) [18] together with the Matched Asymptotic Expansion (MAE) [19]. However, in both cases only the role of a single platelet was considered, and neither of them included the effect of residual stresses.

Therefore, the main objective of this paper is to complete the numerical tool introduced in [17] by incorporating the influence of residual stresses and the volume fraction. For the very first time, this study numerically investigates the impact of these two parameters on fracture toughness, determining which one plays a more significant role. This finding can be particularly valuable for design optimization. The model presented in this paper is illustrated and validated using the numerical and experimental studies previously mentioned.

This paper is divided into 6 sections. In Section 2 the new thermomechanical problem is described, as well as the mechanical properties of the composite. The application of the CC together with the MAE is explained in Section 3 and 4, respectively. Results are shown in Section 5, which is divided in 3 parts. A first part where the effect of residual stresses is analyzed, a second one including the effect of the volume fraction, and a final comparison with results found in the literature. Final conclusions are drawn in Section 6.

2. Description of the problem

Based on the experiments made in [1] and [8], a symmetric 3-point bending test with a pre-existing crack Γ_c under Mode I loading conditions and a cooling change in temperature $\Delta\theta$ is considered, see Fig. 1. At the tip of the pre-existing crack there is a platelet of hexagonal shape oriented a certain angle α,

whose dimensions are, according to experiments, major axe $d = 5 - 25$ μm and thickness $t = 0.2d$. The platelet is immersed in a volume of glass according to the volume fraction V_p, the whole being itself immersed in a homogenized material (see below) called in the following the composite. The major axe and thickness of the glass envelope are a_1 and a_2 and fulfill

$$a_1 = \frac{d}{\sqrt{V_\mathrm{p}}} \qquad \text{and} \qquad a_2 = \frac{t}{\sqrt{V_\mathrm{p}}}. \tag{1}$$

The interface between the platelet and the matrix is assumed to be strong as reported in [9].

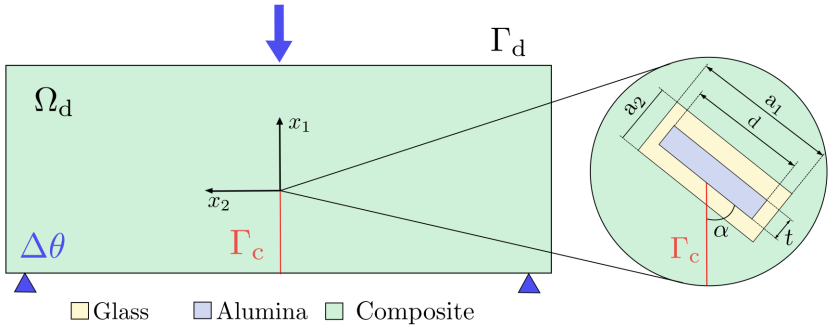

Figure 1: Scheme of a symmetric 3-point bending test on a cracked specimen after cooling. A platelet (blue) and its environment (glass in yellow and homogenized material in green) is located at the tip of the crack.

The material properties of alumina and glass are recalled in Table 1. It can be observed that a range for the alumina strength $\sigma_\mathrm{c}^\mathrm{a}$ and fracture toughness K_IC^a is estimated [17], since these properties in platelets of alumina are very difficult to measure. The smallest and biggest values will be called respectively minor and major in the following. Notice that the superscripts $^\mathrm{a}$ or $^\mathrm{g}$ are used when referring to alumina or glass mechanical properties.

Constituents	E [GPa]	ν	α_{t} [10^{-6}/K]	σ_{c} [MPa]	K_{IC} [MPa m$^{1/2}$]
Borosilicate glass	60	0.23	3.3	56	0.735
Alumina (Al_2O_3)	402	0.22	8.9	$300-400$	$2-5$

Table 1: Mechanical properties of the constituents. The extreme values of the tensile strength and toughness of alumina will be called respectively minor and major in the following.

All around the platelet/glass assembly, a homogeneous distribution of platelets is assumed [8] and therefore the composite is represented through an equivalent homogenized material, whose mechanical properties depend on V_{p} in Table 2. Its Young's modulus E^{app} was measured in [1] and [8], whereas the Poisson's ratio ν^{app} is assumed to be that of glass, since there is not a big difference between Poisson's ratios of alumina ν^{a} and glass ν^{g}, see Table 1.

The thermal expansion coefficient $\alpha_{\mathrm{t}}^{\mathrm{app}}$ for the composite was calculated using Voigt's rule of mixtures [20]. The tensile strength and $\sigma_{\mathrm{c}}^{\mathrm{app}}$ was also measured in [1] and [8]. Finally, two experimental sets of data for the apparent fracture toughness $K_{\mathrm{IC}}^{\mathrm{app}}$ in the composite were included, denoted as [1] referring to [8] and [2] referring to [1], see Table 2.

	E^{app} [GPa]	ν^{app}	$\alpha_{\mathrm{t}}^{\mathrm{app}}$ [10^{-6}/K]	$\sigma_{\mathrm{c}}^{\mathrm{app}}$ [MPa]	$K_{\mathrm{IC}}^{\mathrm{app}}$ [MPa m$^{1/2}$]	
$\mathrm{V_p} = 5\%$	63	0.22	3.58	67	0.98^1	0.9^2
$\mathrm{V_p} = 10\%$	70	0.22	3.86	84	1.03^1	0.95^2
$\mathrm{V_p} = 15\%$	79	0.22	4.14	104	1.28^1	1.1^2
$\mathrm{V_p} = 30\%$	102	0.22	4.98	150	1.92^1	1.5^2

Table 2: Mechanical properties of the equivalent homogenized material for several values of platelets volume fraction V_{p}.

The problem illustrated in Fig. 1 is a thermomechanical one. A superposition principle can be applied to describe the solution $\underline{U}(x_1, x_2)$ as the sum of the solution to a pure mechanical problem $\underline{U}^{\mathrm{cr}}$ and the solution to a thermoelastic

problem $\underline{U}^{\mathrm{te}}$

$$\underline{U}(x_1, x_2) = \underline{U}^{\mathrm{cr}}(x_1, x_2) + \underline{U}^{\mathrm{te}}(x_1, x_2). \tag{2}$$

The pure mechanical problem was already developed in [17] and therefore only the thermoelastic problem is detailed in this paper, its variational formulation is

Find $\underline{U}^{\mathrm{te}} \in \mathcal{W}^{\mathrm{te}}$ such that

$$\int_\Omega \mathbf{C} : \nabla \underline{U}^{\mathrm{te}} : \nabla \underline{\phi}\, dx_1 dx_2 = \int_\Omega \mathbf{C} : \underline{\underline{\varepsilon}}^{\mathrm{in}} : \nabla \underline{\phi}\, dx_1 dx_2, \qquad \forall \underline{\phi} \in \mathrm{H}^1(\Omega), \tag{3}$$

where $\mathrm{H}^1(\Omega)$ denotes the first order Sovolev space. Note that only the smoothness condition is required for the space of admissible solution, since the cooling occurs without any constraint on the boundaries of the specimen. The inelastic strain tensor appearing in (3) is

$$\underline{\underline{\varepsilon}}^{\mathrm{in}} = -\alpha_{\mathrm{t}} \Delta\theta \underline{\underline{I}}, \tag{4}$$

where the temperature change during cooling $\Delta\theta = \theta_0 - \theta_f$ is the difference between the initial temperature θ_0, which corresponds in this case to the glass transition temperature $\theta_0 \approx 550°C$ [11], and the final one θ_f (the room temperature), and $\underline{\underline{I}}$ is the identity matrix.

As in [17], we assume the plane strain elasticity for simplicity, since we are primarily interested in the effects of smallness.

3. Matched asymptotic approach in the thermoelastic problem

In the thermoelastic problem described above the platelet located at the crack-tip is considered a perturbation of Ω_d, since its size is much smaller than the specimen dimensions. Consequently, the MAE can be applied to estimate the elastic displacement $\underline{U}_d^{\mathrm{te}}(x_1, x_2)$ in its vicinity, where the lower index $_d$ is used to emphasize the dependence of the solution on the size of the platelet. In this framework, two expansions are used to approximate $\underline{U}_d^{\mathrm{te}}(x_1, x_2)$. On the

one hand, the outer expansion is written as

$$\underline{U}_d^{\mathrm{te}}(x_1, x_2) = \underline{U}_0^{\mathrm{te}}(x_1, x_2) + \text{small correction}, \tag{5}$$

where $\underline{U}_0^{\mathrm{te}}(x_1, x_2)$ is the solution of the same thermoelastic problem defined in the unperturbed domain Ω_0. It is the macroscopic approach in which it is assumed that the perturbation is too small that it is not appreciable in the specimen which is therefore composed only of the homogenized material. Assuming this homogenized material to be isotropic, the outer solution $\underline{U}_0^{\mathrm{te}}(x_1, x_2)$ can be easily integrated from

$$\underline{\underline{\varepsilon}}_0^{\mathrm{te}}(x_1, x_2) = \underline{\underline{\varepsilon}}^{\mathrm{in}} \; ; \; \underline{\underline{\sigma}}_0^{\mathrm{te}}(x_1, x_2) = \underline{\underline{0}} \tag{6}$$

$$\underline{U_0}^{\mathrm{te}}(x_1, x_2) = \underline{U_0}^{\mathrm{te}}(0, 0) + \underline{\underline{\varepsilon}}^{\mathrm{in}} \left[x_1, x_2\right]^{\mathrm{T}} . \tag{7}$$

This approximation correctly represents $\underline{U}_d^{\mathrm{te}}(x_1, x_2)$ far away from the perturbation. On the other hand, the inner expansion is characterized by a change of variable $x_i = dy_i$ $(i = 1, 2)$ and $r = d\rho$, which defines an unbounded domain Ω_{in}, see Fig. 2. It is expressed as

$$\underline{U}_d^{\mathrm{te}}(x_1, x_2) = \underline{U}_d^{\mathrm{te}}(dy_1, dy_2) = F_0^{\mathrm{te}}(d)\underline{V}_0^{\mathrm{te}}(y_1, y_2) + F_1^{\mathrm{te}}(d)\underline{V}_1^{\mathrm{te}}(y_1, y_2) + ... \tag{8}$$

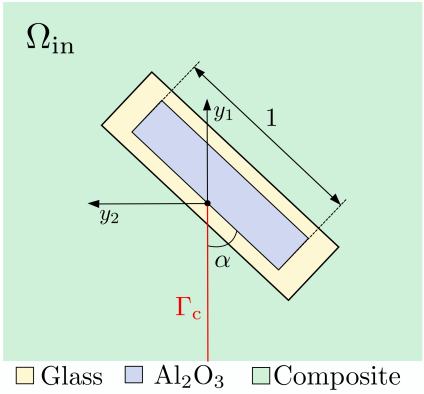

Figure 2: Scheme of the inner domain.

Notice that the inner expansion is a good approximation of the actual solution in the vicinity of the platelet. Terms $\underline{V}_0^{\mathrm{te}}(y_1, y_2)$ and $\underline{V}_1^{\mathrm{te}}(y_1, y_2)$ are defined

through the matching conditions, in which the outer and inner expansion are related in an intermediate region, as it was explained in [17],

$$F_0(d) = 1, \qquad \underline{V}_0^{\mathrm{te}}(y_1, y_2) \sim \underline{U}_0^{\mathrm{te}}(0,0) \qquad \text{when } \rho \to \infty, \tag{9}$$

$$F_1(d) = d, \qquad \underline{V}_1^{\mathrm{te}}(y_1, y_2) \sim \underline{\underline{\varepsilon}}^{\mathrm{in}}\,[y_1, y_2]^T \qquad \text{when } \rho \to \infty, \tag{10}$$

where the symbol $\sim$ means "behaves like". Then, it is obtained that $\underline{V}_0^{\mathrm{te}}(y_1, y_2) = \underline{U}_0^{\mathrm{te}}(0,0)$. The term $\underline{V}_1^{\mathrm{te}}(y_1, y_2)$ is numerically obtained using FEM on a very large but bounded domain with a traction free condition along the artificial outer boundary (6). Therefore,

$$\underline{U}_d^{\mathrm{te}}(x_1, x_2) = \underline{U}_0^{\mathrm{te}}(0,0) + d\ \underline{V}_1^{\mathrm{te}}(y_1, y_2) + ... \tag{11}$$

On the other hand, the actual stress tensor $\underline{\underline{\sigma}}_d^{\mathrm{te}}$ can be expressed in terms of the stress tensor in the inner problem,

$$\underline{\underline{\sigma}}_d^{\mathrm{te}}(x_1, x_2) = \underline{\underline{\sigma}}_d^{\mathrm{te}}(dy_1, dy_2) = \mathbf{C} : \left(\nabla_y \underline{V}_1^{\mathrm{te}}(y_1, y_2) - \underline{\underline{\varepsilon}}^{\mathrm{in}}\right) + \text{small correction} \tag{12}$$

In addition, let us recall the outer and inner expansions of the elastic problem (refer to [17] for the exact meaning of the terms which, however, can be understood quite easily),

$$\begin{aligned}
&\text{The outer expansion} \\
&\underline{U}_d^{\mathrm{cr}}(x_1, x_2) = \underline{U}_0^{\mathrm{cr}}(x_1, x_2) + \text{small correction} \\
&\text{with the Williams' expansion} \\
&\underline{U}_0^{\mathrm{cr}}(x_1, x_2) = \underline{U}_0^{\mathrm{cr}}(0,0) + K_{\mathrm{I}}\ r^{1/2}\ \underline{u}_{\mathrm{I}}(r, \theta) + ... \\
&\text{and the inner expansion} \\
&\underline{U}_d^{\mathrm{cr}}(x_1, x_2) = \underline{U}_0^{\mathrm{te}}(0,0) + K_{\mathrm{I}}\ \sqrt{d}\ \underline{V}_1^{\mathrm{cr}}(y_1, y_2) + ...
\end{aligned} \tag{13}$$

We should theoretically include the T-stress in these expansions to be consistent with (7), but, after trying, it turns out that its influence is negligible in all cases.

4. The coupled criterion in a heterogenous structure

The crack nucleation and propagation can be predicted by the CC, defined by two necessary and sufficient conditions: a stress and an energy conditons [21]. Considering a heterogeneous structure with N different materials, the stress condition is written as a function of the tensile stress $\sigma(s)$ along the expected crack path (i.e. prior to any crack extension), using s as a coordinate (plane strain assumption),

$$\bar{\sigma} = \frac{\sigma(s)}{\sigma_{\mathrm{c}}(s)} \geq 1 \qquad \text{for } 0 \leq s \leq \delta l. \tag{14}$$

being δl the newly created crack length. The tensile strength $\sigma_{\mathrm{c}}(s)$ is defined as

$$\sigma_{\mathrm{c}}(s) = \sum_{i=1}^{N} \sigma_{\mathrm{c}}^{i} \left[H(s - \delta l_{i-1}) - H(s - \delta l_i) \right], \tag{15}$$

where H is the Heaviside function and $\delta l_0 = 0$. Notice that $N = 3$ is the problem represented in Fig. 1, whereas $N = 2$ is used if only a single platelet embedded in a glass matrix is studied [17]. The stress condition in the thermomechanical problem (2) is therefore described as

$$\bar{\sigma} = \frac{\sigma^{\mathrm{cr}}(s) + \sigma^{\mathrm{te}}(s)}{\sigma_{\mathrm{c}}(s)} \geq 1 \qquad \text{for} \qquad 0 \leq s \leq \delta l, \tag{16}$$

The energy condition is based on an energy balance between the change in potential and kinetic energy, $\Delta\Pi_{\mathrm{p}}$ and $\Delta\Pi_{\mathrm{k}}$ respectively, and the fracture energy for each material i, $G_{\mathrm{c}}^{i} S_i$,

$$\Delta\Pi_{\mathrm{p}} + \Delta\Pi_{\mathrm{k}} + \sum_{i=1}^{N} G_{\mathrm{c}}^{i} S_i = 0, \tag{17}$$

where S_i is the newly created crack surface and G_{c}^{i} is the critical energy release rate in each material i. In a bidimensional case, this balance holds per unit thickness of the specimen,

$$\Delta\Pi_{\mathrm{p}} + \Delta\Pi_{\mathrm{k}} + \sum_{i=1}^{N} G_{\mathrm{c}}^{i} \delta l_i = 0, \tag{18}$$

and δl_i denotes the newly created crack length within each material i. Assuming the initial state to be quasi-static, $\Delta\Pi_{\mathrm{k}} \geq 0$, the energy condition can be written as

$$\bar{G}_{\mathrm{inc}} = -\frac{\Delta\Pi_{\mathrm{p}}(\delta l)}{\delta l} \cdot \frac{1}{G_{\mathrm{c}}(\delta l)} \geq 1, \tag{19}$$

where the parameter $G_{\mathrm{c}}(\delta l)$ is

$$G_{\mathrm{c}}(\delta l) = \frac{\sum_{i=1}^{N} G_{\mathrm{c}}^{i} \delta l_i}{\delta l}, \tag{20}$$

in which $\delta l = \sum_{i=1}^{N} \delta l_i$. The change in potential energy $\Delta\Pi_{\mathrm{p}}(\delta l) = \Delta W(\delta l)$, being W the total strain energy in the system defined as

$$W(\delta l) = \frac{1}{2} \int_{\Omega} \mathbf{C} : (\nabla \underline{U} - \underline{\underline{\varepsilon}}^{\mathrm{in}}) : (\nabla \underline{U} - \underline{\underline{\varepsilon}}^{\mathrm{in}})\, dx_1 dx_2, \tag{21}$$

Using the superposition principle of the thermomechanical problem (2) it comes out,

$$W(\delta l) = \frac{1}{2} \int_{\Omega} \mathbf{C} : \left(\nabla \underline{U}^{\mathrm{cr}} + \nabla \underline{U}^{\mathrm{te}} - \underline{\underline{\varepsilon}}^{\mathrm{in}}\right) : \left(\nabla \underline{U}^{\mathrm{cr}} + \nabla \underline{U}^{\mathrm{te}} - \underline{\underline{\varepsilon}}^{\mathrm{in}}\right) dx_1 dx_2. \tag{22}$$

Considering (3), the strain energy in the system is rewritten as

$$\begin{aligned} W(\delta l) = \frac{1}{2} \int_{\Omega} \mathbf{C} : \nabla \underline{U}^{\mathrm{cr}} : \nabla \underline{U}^{\mathrm{cr}} dx_1 dx_2 - \frac{1}{2} \int_{\Omega} \mathbf{C} : \nabla \underline{U}^{\mathrm{te}} : \nabla \underline{U}^{\mathrm{te}}\, dx_1 dx_2 \\ + \frac{1}{2} \int_{\Omega} \mathbf{C} : \underline{\underline{\varepsilon}}^{\mathrm{in}} : \underline{\underline{\varepsilon}}^{\mathrm{in}}\, dx_1 dx_2 = W^{\mathrm{cr}} - W^{\mathrm{te}} + W^{\mathrm{in}}. \end{aligned} \tag{23}$$

Since we are interested in the increment in strain energy, $\Delta W(\delta l) = W(\delta l) - W(0)$, the last term W^{in} in the previous expression does not play any role in the energy condition, then

$$\bar{G}_{\mathrm{inc}} = -\frac{\Delta\Pi_{\mathrm{p}}}{\delta l} \cdot \frac{1}{G_{\mathrm{c}}(\delta l)} = \left(-\frac{\Delta W^{\mathrm{cr}}}{\delta l} + \frac{\Delta W^{\mathrm{te}}}{\delta l}\right) \cdot \frac{1}{G_{\mathrm{c}}(\delta l)} \geq 1. \tag{24}$$

note that there is no coupling term in (23), this a consequence of the boundary conditions and the variational formulation of the problems. In this problem, the actual solution is approximated using the MAE. In [17] it was explained how the tensile stress σ^{cr} and the increment in strain energy ΔW^{cr} were obtained in the mechanical problem using MA approach. In the thermoelastic problem the

tensile stress σ^{te} is calculated applying (12), and the increment in strain energy ΔW^{te} is expressed as

$$\Delta W^{\mathrm{te}} = d\,\Delta\hat{W}^{\mathrm{te}}. \tag{25}$$

where $\Delta\hat{W}^{\mathrm{te}}$ is the increment in strain energy in the inner thermoelastic problem. Considering that $\hat{\sigma}^{\mathrm{te}}(\hat{s})$ and $\hat{W}^{\mathrm{te}}$ the thermoelastic solution for $\Delta\theta = 1$, the CC is therefore expressed for a general value of $\Delta\theta$ as

$$\bar{\sigma} = \frac{\dfrac{K_{\mathrm{I}}}{\sqrt{d}}\,\hat{\sigma}^{\mathrm{cr}}(\hat{s}) + \Delta\theta\hat{\sigma}^{\mathrm{te}}(\hat{s})}{\sigma_c(\hat{s})} \geq 1, \quad \text{for } 0 \leq \hat{s} \leq \delta l^{\mathrm{in}} \tag{26}$$

$$\bar{G}_{\mathrm{inc}} = \frac{-(K_{\mathrm{I}})^2\,\dfrac{\Delta\hat{W}^{\mathrm{cr}}}{\delta l^{\mathrm{in}}} + d\,\Delta\theta^2\dfrac{\Delta\hat{W}^{\mathrm{te}}}{\delta l^{\mathrm{in}}}}{G_{\mathrm{c}}(\delta l^{\mathrm{in}})} \geq 1. \tag{27}$$

where $\hat{s} = s/d$. The aim of applying the CC is to calculate the apparent fracture toughness of the composite $K_{\mathrm{IC}}^{\mathrm{app}}$, defined as the minimum value of K_{I} for which both the stress (26) and the energy (27) condition are fulfilled. In particular, $K_{\mathrm{IC}}^{\mathrm{app}}$ is compared to $K_{\mathrm{IC}}^{\mathrm{g}}$, the fracture toughness of glass, to study how glass fracture properties are enhanced when a second constituent (in this case, alumina) is added.

At this stage, we must point out an important difficulty encountered by the numerical approach of the CC. There is a singularity at the tip of the mother crack impinging the matrix/platelet interface and, despite it is located at the tip of a crack, it differs from the singularity for a crack in the classical theory of Linear Elastic Fracture Mechanics $\lambda = 0.5$, because of the heterogeneous conditions [22]. The platelet being stiffer than the matrix, it is a so-called weak singularity with an exponent larger than that of a crack. If the mechanical loading (bending) leads to a positive generalized stress intensity factor (GSIF) of the singularity, on the contrary, the residual stresses tend to close the mother crack and result in a negative GSIF. There is a competition between them, if the GSIF related to a mechanical load is small, then residual stresses take over and the mother crack remains closed. Unfortunately, all this happens in a very small neighborhood of the crack tip, where the stress variations are difficult to

capture numerically due to the singularity, and therefore the calculations are very mesh dependent.

A way to get rid of this difficulty is to compute the two GSIFs. First, the GSIF referred to the mechanical problem, $k^{\rm cr}$, is extracted from $\underline{U}_d^{\rm cr}$ using the path independent integral described in [19]

$$k^{\rm cr} = \frac{\Psi(\underline{U}_d^{\rm cr}, r^{-\lambda}\,\underline{u}^-(\theta))}{\Psi(r^{\lambda}\,\underline{u}(\theta), r^{-\lambda}\,\underline{u}^-(\theta))}, \tag{28}$$

where $r^{\lambda}\,\underline{u}(\theta)$ is the eigenfunction of the heterogeneous problem, being $r^{-\lambda}\,u^-(\theta)$ the dual eigenfunction. For the GSIF referred to the thermoelastic problem ($k^{\rm te}$) the right-hand side member in (3) does not vanish in the vicinity of the singular point, and consequently the integral Ψ is no longer a path-independent integral. A superposition principle might be used to separate the non-homogeneous part of $\underline{U}_d^{\rm te}$, and therefore to calculate $k^{\rm te}$.

The inner solution obtained using MAE can be used in the calculation of $k^{\rm cr}$ and $k^{\rm te}$. First, the GSIF's $\kappa^{\rm te}$ and $\kappa^{\rm cr}$ are extracted respectively from $\underline{V}_1^{\rm te}$ and $\underline{V}_1^{\rm cr}$. Then, the corresponding changes are applied using (11) and (13) to obtain the GSIF's of the actual problem,

$$k^{\rm te} = d^{1-\lambda}\Delta\theta\ \kappa^{\rm te} \tag{29}$$

$$k^{\rm cr} = K_{\rm I}\ d^{1/2-\lambda}\ \kappa^{\rm cr}. \tag{30}$$

Then, equality $k^{\rm cr} = -k^{\rm te}$ provides the smaller value $K_{\rm I}^{\rm min}$ of $K_{\rm I}$ such that there is not a compressive stress and the mother crack opens.

$$K_{\rm I}^{\rm min} = \sqrt{d}\Delta\theta\ \frac{\kappa^{\rm te}}{\kappa^{\rm cr}}. \tag{31}$$

It is a lower bound of admissible $K_{\rm I}$. Numerically, the fact that $\kappa^{\rm cr}$ outweighs $\kappa^{\rm te}$, is tricky to detect as already mentioned. We have opted for a check of the convexity of $\bar{\sigma}(s)$ as function of s at the first computation points. Hence, the first and the second derivative of $\bar{\sigma}(s)$ have been checked in the neighbourhood of the singularity (at $s = 0$). The first derivative must be negative for a decreasing function and the second derivative must be positive to obtain a convex evolution of $\bar{\sigma}(s)$.

5. Results

This section is divided into 3 parts. First, in subsection 5.1 the influence of residual stresses is studied without including the effect of the volume fraction, i.e., considering the role of a single platelet in the thermomechanical problem. Then, in subsection 5.2 the volume fraction together with residual stresses is analysed. Finally, in subsection 5.2.3 a comparison with experimental results extracted from literature is made to ensure that the model is consistent. Results are exhibited for different platelet sizes, at the scale of experiments carried out in [1, 8], i.e. $d = 5 - 25\,\mu$m and at an extended scale $d = 3 - 300\,\mu$m used to better capture the size effect on the apparent fracture toughness. Moreover, two orientations of the platelet are studied, $\alpha = 90°$ and $\alpha = 0°$. The selection of these two orientations is based on the numerical study made in [16]. In the former several expected crack path are analysed, to determine which one governs the pre-existing crack propagation: a penetration in the platelet, a decohesion at the end of the platelet and a deviation along the interface matrix/platelet. In the Fig. 3 a scheme of these mechanisms is shown.

Therefore, in this section the influence of different parameters (d, α, $\Delta\theta$ and V_{p}) is investigated in order to determine when these factors contribute to enhance the apparent fracture toughness of the composite, $K_{\mathrm{IC}}^{\mathrm{app}}$.

5.1. Influence of residual stresses. The role of a single platelet

In case of a single platelet, the model considers only two components, alumina and glass, the homogenized material is nothing but glass. For a cooling down $\Delta\theta = 500$ K, the influence of the parameter d in the implementation of the CC is analysed. Results are also compared with the case where there are no residual stresses.

5.1.1. Angle $\alpha = 90°$

When the platelet is perpendicular to the pre-existing crack, the expected crack growth is not known a priori and several possibilities might be analysed [17]: penetration, decohesion and deflection, see Fig. 3.

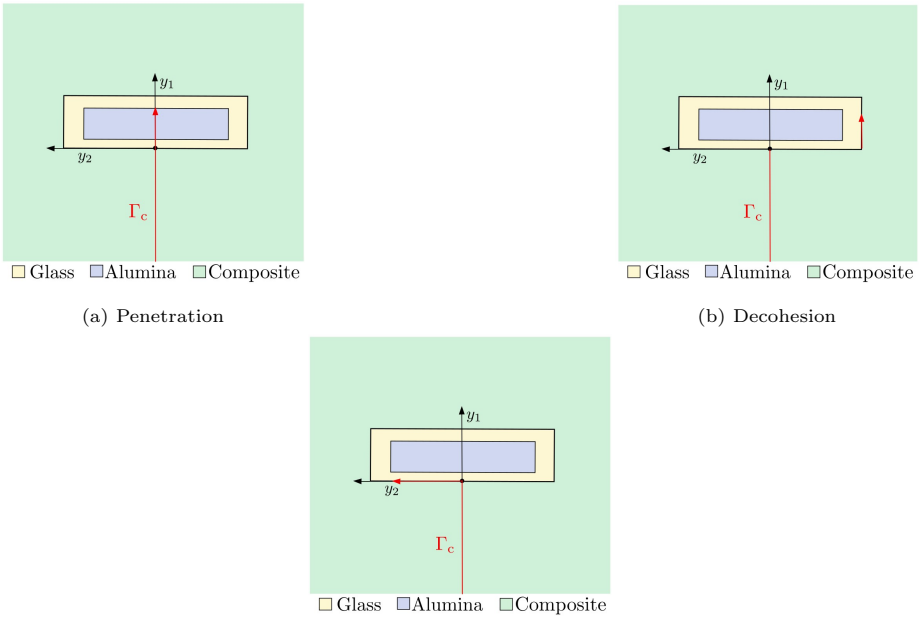

(a) Penetration

(b) Decohesion

(c) Deflection

Figure 3: Schematic view of the inner domain and the expected crack path when $\alpha = 90°$.

For penetration (Fig. 3a) two scenarios are examined, called minor and major, corresponding to the minor and major values of alumina strength and toughness in Table 1. These two scenarios have been named penetration major and minor for the sake of simplicity. As shown in Fig. 4, both converge to the same values of $K_{\mathrm{IC}}^{\mathrm{app}}$ for $d > 150$ μm, which means that alumina fracture properties play no longer a role in the damage propagation. The reason is that for $d > 150$ μm it is the mother crack opening condition which prevails, while, for $d < 150$ μm they do play a role, the greater the alumina fracture properties, the higher $K_{\mathrm{IC}}^{\mathrm{app}}$. It is compared to $K_{\mathrm{I}}^{\mathrm{min}}$ and, as expected, both curves are above.

Moreover, for $\alpha = 90°$ the singularity exponent in the heterogeneous problem is a real number $\lambda = 0.638$, and therefore our numerical calculations can be compared to $K_{\mathrm{I}}^{\mathrm{min}}$. As expected, both curves are above.

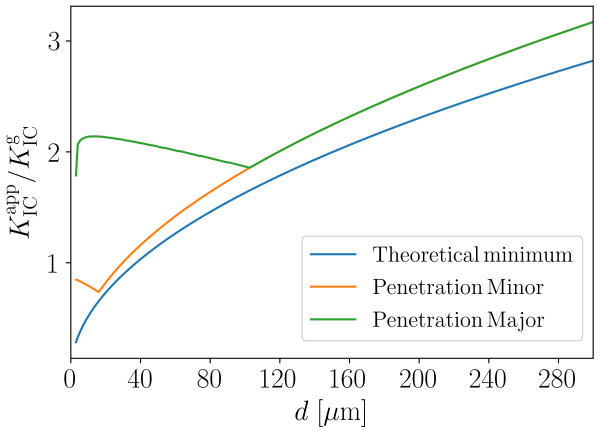

Figure 4: Comparison between the theoretical minimum $K_{\mathrm{I}}^{\mathrm{min}}$ and the apparent fracture toughness $K_{\mathrm{IC}}^{\mathrm{app}}$ obtained for the major and the minor values of alumina strength and toughness (see Table 1), for the penetration case.

The same comparison is carried out for the deflection mechanism (Fig. 3c) with similar conclusions (Fig. 5).

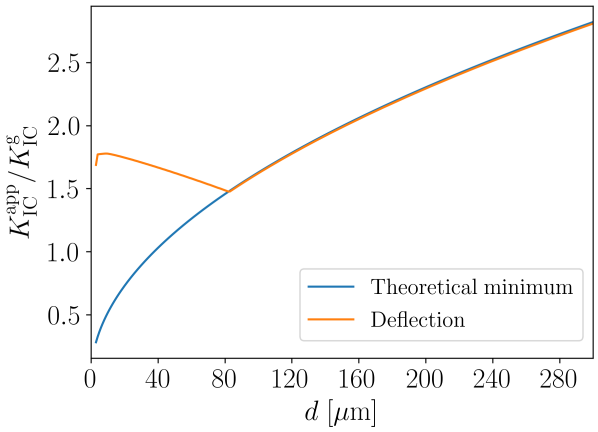

Figure 5: Comparison between the theoretical minimum $K_{\mathrm{I}}^{\mathrm{min}}$ and the apparent fracture toughness $K_{\mathrm{IC}}^{\mathrm{app}}$ obtained for the deflection case.

In the decohesion case (Fig. 3b), the situation is slightly different because

the crack does not initiate at the mother crack tip but at the corner of the platelet (which undergoes also a singularity), then this mechanism can occur even if the mother crack is closed. The only point to check is the opening or not of the pre-existing crack to be sure that the appropriate boundary conditions prevail along the crack faces. It has been checked that it is either opened or fully closed.

The three cases are compared in Fig. 6. The actual apparent fracture toughness is the minimum value of $K_{\mathrm{IC}}^{\mathrm{app}}$ among the three curves which corresponds to the predominant mechanism. It can be pointed out that $K_{\mathrm{IC}}^{\mathrm{app}}$ is lower than $K_{\mathrm{IC}}^{\mathrm{g}}$ for long platelets $d > 98$ μm. In fact, for $d > 132$ μm the CC predicts a breakage by a lateral decohesion during cooling, which agrees with experimental observations [11].

For short platelets $d < 98$ μm the toughening effect depends on alumina fracture properties. In the major case the predominant toughening mechanism is either decohesion or deflection, and $K_{\mathrm{IC}}^{\mathrm{app}} > K_{\mathrm{IC}}^{\mathrm{g}}$ in the whole range. In the minor case, $K_{\mathrm{IC}}^{\mathrm{app}} > K_{\mathrm{IC}}^{\mathrm{g}}$ only for $d = 51 - 98$ μm, and the governing mechanism is either a penetration or a decohesion. In both the major and the minor cases, there is an optimal platelet size that corresponds to the highest value of the actual $K_{\mathrm{IC}}^{\mathrm{app}}$ for each case (Fig. 6).

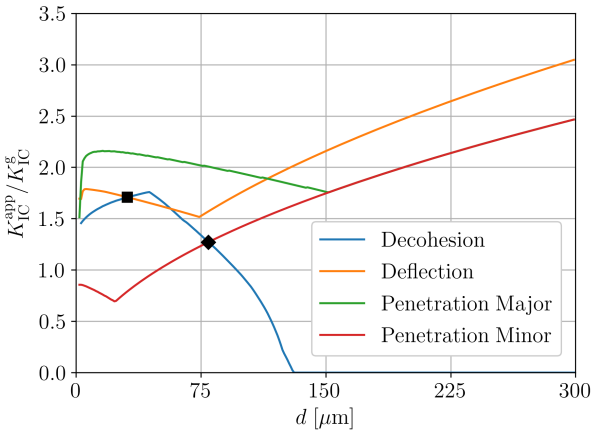

Figure 6: Comparison between decohesion, deflection, penetration minor and major, for $\alpha = 90°$ and $\Delta\theta = 500\,K$. The diamond and the square correspond to the optimal points in the minor and the major case respectively .

The influence of residual stresses at the scale of experiments $d = 5 - 25$ μm is studied in Fig. 7, where the apparent fracture toughness of the composite is compared for $\Delta\theta = 0$ K (no residual stresses) and $\Delta\theta = 500$ K. In the major case a slight enhancement of $K_{\mathrm{IC}}^{\mathrm{app}}$ with respect to $K_{\mathrm{IC}}^{\mathrm{g}}$ is observed, whereas in the minor case it is shown that residual stresses do not enhance the toughness, since $K_{\mathrm{IC}}^{\mathrm{app}} < K_{\mathrm{IC}}^{\mathrm{g}}$ in the whole range. The predominant mechanism does not change with $\Delta\theta$, being a lateral decohesion in the major case, which agrees with predictions made in [12], and a penetration for the minor case.

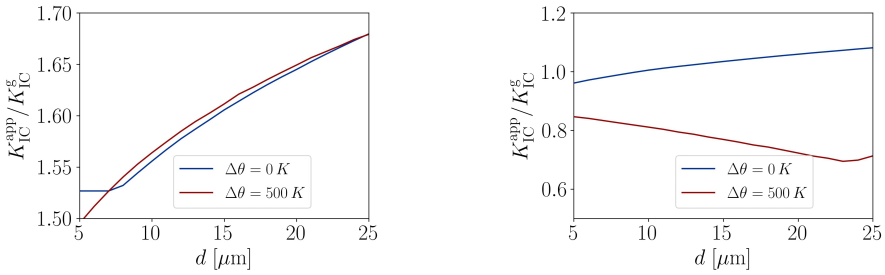

(a) Major case

(b) Minor case

Figure 7: Influence of $\Delta\theta$ on K_{IC}^{app} for $\alpha = 90°$ at the scale of experiments.

Furthermore, the influence of residual stresses is also analysed for an extended range of the platelet size $d = 3 - 300$ μm in Fig. 8, where it is clearly observed that residual stresses reduce the apparent fracture toughness when considering very long platelets. In both cases residual stresses promote a lateral decohesion as the predominant mechanism, specially for long platelets.

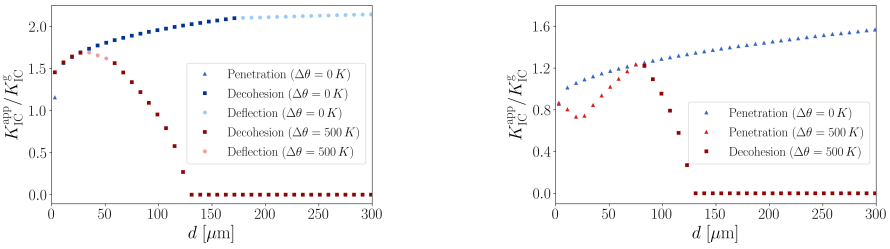

(a) Major case

(b) Minor case

Figure 8: Influence of $\Delta\theta$ on K_{IC}^{app} for $\alpha = 90°$ in an extended range of d. The square, circular and triangular symbols represent decohesion, deflection and penetration, respectively.

5.1.2. Angle $\alpha = 0°$

When the platelet is aligned with the pre-existing crack, $\alpha = 0°$, a crack growth through the interface glass/alumina is expected, as shown in Fig. 9.

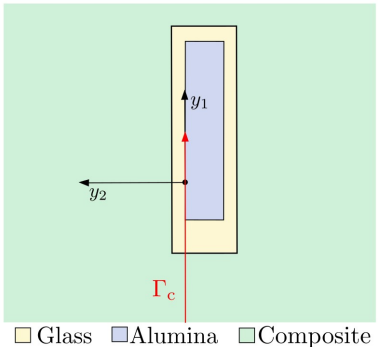

Figure 9: Schematic view of the inner domain and the expected crack path when $\alpha = 0°$

The difficulty described in Section 4 is still present and even worsen insofar as the exponent of the crack tip singularity impinging the corner of the platelet is a complex number, $\lambda \pm \mathrm{i}\ \varepsilon = 0.535 \pm \mathrm{i}\ 0.054$. The same complex character holds for the GSIFs κ^{te} and κ^{cr} which can however still be extracted from $\underline{V}_1^{\mathrm{te}}$ and $\underline{V}_1^{\mathrm{cr}}$ using again the path independent integral described in [19], [23, 24]. And this is still true for the actual GSIFs k^{te} and k^{cr} derived from (11)) and (13) through (29) and (30). However, contrary to the previous case, it is thus impossible to compare them to know if the mechanical loading prevails on the residual stresses. However, it can be noted that because of the smallness of the imaginary part ε of the singular exponent, the oscillations inherent in this kind of solutions develop on such a small scale that they have no physical significance. Then, (31) can be replaced by a condition of decrease and convexity of the tensile stress associated with the singular terms to define $K_{\mathrm{I}}^{\mathrm{min}}$. In other words, we determine the value of $K_{\mathrm{I}}^{\mathrm{min}}$ considering that $\bar{\sigma}(s)$ in the vicinity of the singularity must be a decreasing and convex function.

The effect of residual stresses and the platelet size on $K_{\mathrm{IC}}^{\mathrm{app}}$ is studied in Fig. 10 for $\Delta\theta = 0$ K and $\Delta\theta = 500$ K, at the two families of scales described in the previous section, $d = 5-25$ μm and $d = 3-300$ μm. Clearly, a toughening effect ($K_{\mathrm{IC}}^{\mathrm{app}} > K_{\mathrm{IC}}^{\mathrm{g}}$) is never observed at the experimental scale, with and without residual stresses, as shown in Fig. 10a. In fact, residual stresses reduce the apparent fracture toughness in the composite. Interestingly, when considering

an extended scale, see Fig. 10b, $K_{\mathrm{IC}}^{\mathrm{app}}$ is higher than $K_{\mathrm{IC}}^{\mathrm{g}}$ for $d > 60\,\mu$m, for both $\Delta\theta = 0$ K and 500 K. In the latter, two different evolution of $K_{\mathrm{IC}}^{\mathrm{app}}$ are observed. For $d < 36$ μm $K_{\mathrm{IC}}^{\mathrm{app}}$ is decreasing and the energy condition is governing the failure, otherwise $K_{\mathrm{IC}}^{\mathrm{app}}$ is increasing and the stress condition is governing. In the latter the crack growth is determined by the negative thermal GSIF in the thermoelastic problem.

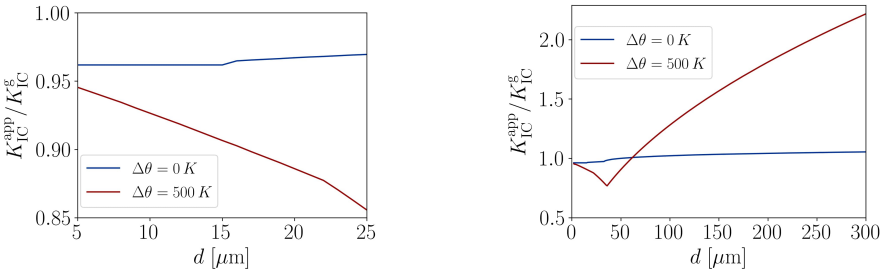

(a) Scale of experiments

(b) Extented scale

Figure 10: Influence of $\Delta\theta$ and d on $K_{\mathrm{IC}}^{\mathrm{app}}$ for $\alpha = 0°$ and $V_{\mathrm{p}} = 0\%$.

5.2. Influence of the volume fraction

The mechanical properties of the equivalent homogenized material depend on the volume fraction V_{p}. The values chosen for this study correspond to the ones found in the literature [1], $V_{\mathrm{p}} = 0\,\%$, $5\,\%$, $10\,\%$, $15\,\%$ and $30\,\%$ (note that $0\,\%$ means a single platelet by abuse of notation). As in Section 5.1, two orientations of the platelet have been studied, $\alpha = 0°$ and $\alpha = 90°$.

5.2.1. Angle $\alpha = 90°$

The case of $\alpha = 90°$ requires the analysis of three different crack paths described in Section 5.1.1: deflection, decohesion and penetration.

First, Fig. 11 shows the influence of V_{p} and d on $K_{\mathrm{IC}}^{\mathrm{app}}$ in the major case at scale of experiments for $\Delta\theta = 0\,K$ and $500\,K$. In general, a greater toughening effect is observed when increasing V_{p}, whereas little differences related to $\Delta\theta$ are noticed.

As shown in Fig. 11a, for $\Delta\theta = 0\,K$ and $V_\mathrm{p} = 0\,\%$ the predominant mechanism is a lateral decohesion, except for $d = 5\,\mu$m, where it is the penetration. On the other hand, for $V_\mathrm{p} > 0\,\%$, the deflection mostly governs the failure. Only in case of $V_\mathrm{p} = 10\,\%$ and $d = 5\,\mu$m the governing mechanism changes to penetration. Interestingly, intermediate values of the volume fraction $V_\mathrm{p} = 5\,\%$ and $10\,\%$ show values of $K_\mathrm{IC}^\mathrm{app}$ closer to each other. For instance, for $d = 5\ \mu$m and $V_\mathrm{p} = 10\,\%$ the predominant mechanism changes to penetration, and $K_\mathrm{IC}^\mathrm{app}$ is very similar to the one for $V_\mathrm{p} = 5\,\%$.

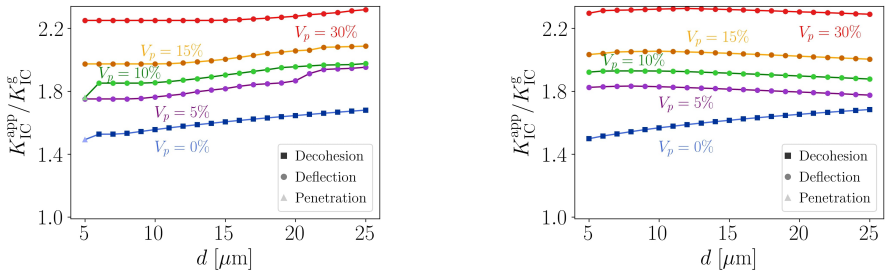

(a) $\Delta\theta = 0\,K$ (b) $\Delta\theta = 500\,K$

Figure 11: Influence of V_p and $\Delta\theta$ on $K_\mathrm{IC}^\mathrm{app}$ at the scale of experiments for $\alpha = 90°$, considering the major case of alumina fracture properties.

Moreover, for $d > 18\,\mu$m and $V_\mathrm{p} = 5\,\%$ there is a jump in $K_\mathrm{IC}^\mathrm{app}$, and it becomes closer to the one obtained for $V_\mathrm{p} = 10\,\%$. This jump also exists for $V_\mathrm{p} > 5\,\%$, but it is not visualized in Fig. 11a because it is located out of the scale of experiments. The reason why this jump occurs is a change in the crack increment predicted by the CC. For platelets larger than $18\,\mu$m the crack jump ends outside the interface glass/alumina, otherwise it remains inside. An example is shown in Fig. 12, where the CC is applied for $d = 25\,\mu$m. The two dimensionless curves $\bar{\sigma}$ and $\bar{G}_\mathrm{inc}$ are represented in Fig. 12a as well as the crack opening when $K_\mathrm{I} = K_\mathrm{IC}^\mathrm{app}$, in Fig. 12b. It can be observed that in this case the crack grows inside the interface glass/alumina until $s = 11.39\,\mu$m. Notice that at the end of the interface glass alumina there is a stress peak due to the singularity at the corner point.

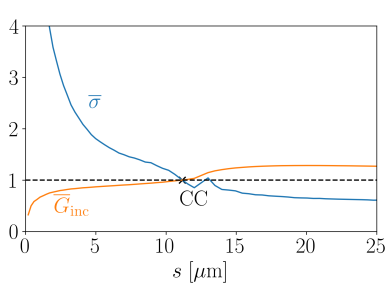

(a) CC curves

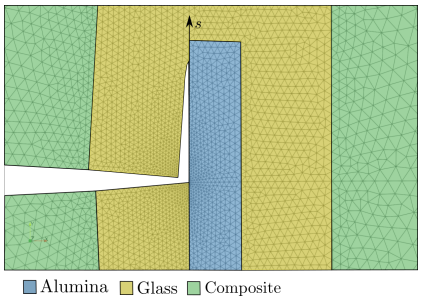

(b) Crack opening

Figure 12: Example of the application of the Coupled Criterion for $d = 25\,\mu$m, $\Delta\theta = 0\,K$ and $V_{\text{p}} = 5\,\%$

Fig. 11b shows the case of $\Delta\theta = 500\,K$, where it can be observed that penetration is no longer a predominant mechanism at the scale of experiments. Instead, the predominant mechanism switches from the lateral decohesion ($V_{\text{p}} = 0\,\%$) to deflection ($V_{\text{p}} > 0\,\%$).

Similar conclusions can be obtained in the minor case represented in Fig. 13. The volume fraction has a greater influence on the apparent fracture toughness than residual stresses. Indeed, in this case residual stresses are not a toughening mechanism, since they reduce the value of $K_{\text{IC}}^{\text{app}}$. Penetration is the predominant mechanism in both cases, with and without thermal effects, i.e., if the alumina fracture properties are not great enough the pre-existing crack always penetrates the platelet. This observation agrees with experimental observations for large intersection angles shown in [8]. Moreover, $K_{\text{IC}}^{\text{app}}$ in the minor case is lower than $K_{\text{IC}}^{\text{app}}$ in the major case.

It is worth mentioning the cases $V_{\text{p}} = 0\,\%$ and $5\,\%$ for $\Delta\theta = 500\,K$ shown in Fig. 13b, where there is a change in the trend of $K_{\text{IC}}^{\text{app}}$ at $d \approx 22.5\,\mu$m, explained by a change in the crack opening. For platelets smaller than $d = 22.5\,\mu$m the crack penetrates at the moment of failure into the alumina until it is arrested inside the glass region, whereas for $d > 22.5\,\mu$m the crack growth stops before reaching the end of the platelet. A similar phenomenon can be observed in Fig. 13a for very short platelets in the case of $V_{\text{p}} = 30\,\%$ and $\Delta\theta = 0\,K$.

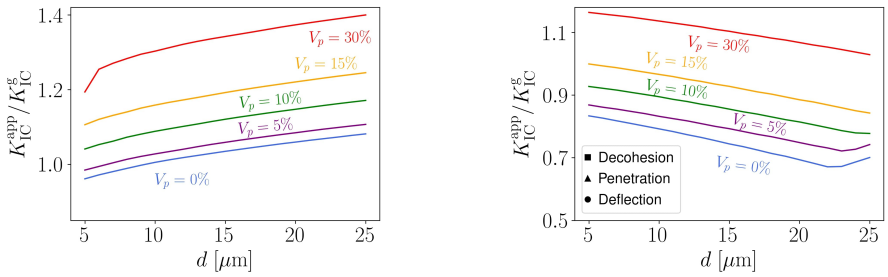

(a) $\Delta\theta = 0\,K$

(b) $\Delta\theta = 500\,K$

Figure 13: Influence of V_p and $\Delta\theta$ on $K_\mathrm{IC}^\mathrm{app}$ at the scale of experiments for $\alpha = 90°$, considering the minor case of alumina fracture properties.

Fig. 14 shows the influence of V_p and the platelet size for an extended range $d = 3 - 300\ \mu$m and the major case of alumina fracture properties, omitting the effect of residual stresses ($\Delta\theta = 0\,K$). Different shapes can be observed in the behaviour of $K_\mathrm{IC}^\mathrm{app}(d)$. For high concentrations of alumina $V_\mathrm{p} > 10\,\%$, where the predominant toughening mechanism is always deflection, the behaviour of the curves is related to a change in the crack opening, depending on the platelet size. For short platelets ($d < 40\,\mu$m) the crack grows until the end of the interface glass alumina at the moment of failure, whereas for longer platelets the crack is arrested before reaching the end of the interface. For low concentrations of alumina $V_\mathrm{p} \leq 10\,\%$ different toughening mechanisms are observed. First, for very short platelets ($d < 5\,\mu$m) the penetration is governing the failure, whereas for very long platelets ($d > 180\,\mu$m) it is always deflection. For an intermediate range ($d = 5 - 180\,\mu$m) of the platelet size the concentration of alumina highly promotes deflection as a toughening mechanism. Hence, for $V_\mathrm{p} = 0\,\%$ it is a lateral decohesion in the whole range, whereas this range is much smaller when increasing V_p.

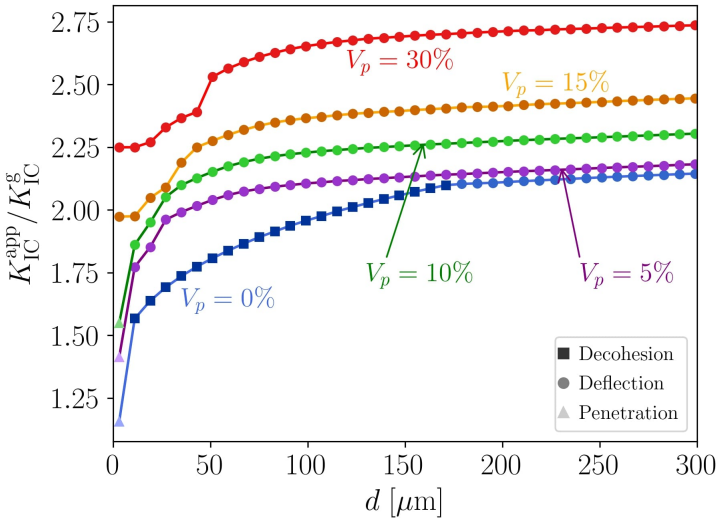

Figure 14: Effect of V_{p} on $K_{\mathrm{IC}}^{\mathrm{app}}$ at the extended scale for $\Delta\theta = 0\,K$ and $\alpha = 90°$, considering the major case of alumina fracture properties.

The effect of residual stresses is analysed in Fig. 15. First, it is observed that for very long platelets the crack grows in a lateral decohesion after cooling without mechanical loads, since $K_{\mathrm{IC}}^{\mathrm{app}} = 0$. This happens when the platelet size is higher than a threshold that increases with growing V_{p}. Indeed, the phenomenon is no longer observed in the selected range of d for $V_{\mathrm{p}} = 30\,\%$, although a strong reduction of $K_{\mathrm{IC}}^{\mathrm{app}}$ can be noticed.

In general, the combination of two effects is shown in Fig. 15. On the one side, the presence of residual stresses promotes decohesion as a predominant mechanism, as it was already mentioned in Section 5.1.1. On the other hand, deflection is more likely to occur for a higher concentration of platelets (i.e. a higher V_{p}). Moreover, for $V_{\mathrm{p}} \geq 10\,\%$ a jump in $K_{\mathrm{IC}}^{\mathrm{app}}$ is observed, generated by a change in the crack opening. For instance, for $V_{\mathrm{p}} = 30\,\%$ and $d < 202\,\mu$m, governed by deflection, the crack grows until a point either outside of the interface alumina glass if $d < 4\,\mu$m, or located at the end of the interface if $d = 4{-}147\,\mu$m, or inside the interface $d > 148\,\mu$m.

Interestingly, when including residual stresses $K_{\mathrm{IC}}^{\mathrm{app}}$ is no longer increasing with the platelet size, except for very short platelets or intermediate size and high concentration of alumina($V_{\mathrm{p}} = 30\,\%$). For this reason, an optimal design point for each V_{p} can be defined, as it was done in Fig. 6. For the sake of simplicity, they have not been highlighted in Fig. 15, but an example of the optimal platelet size for $V_{\mathrm{p}} = 30\,\%$ is $d = 12\,\mu$m, which gives $K_{\mathrm{IC}}^{\mathrm{app}} = 2.32 K_{\mathrm{IC}}^{\mathrm{g}}$.

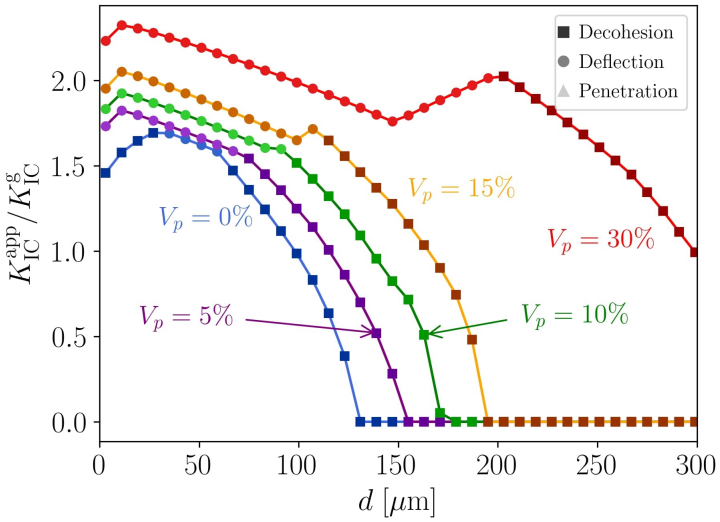

Figure 15: Effect of V_{p} on $K_{\mathrm{IC}}^{\mathrm{app}}$ at the extended scale for $\Delta\theta = 500\,K$ and $\alpha = 90°$, considering the major case of alumina fracture properties.

5.2.2. Angle $\alpha = 0°$

Fig. 16 shows the influence of V_{p} with and without residual stresses, when the platelet is parallel to the pre-existing crack, see Fig. 9. It can be observed that V_{p} has a scaling effect on $K_{\mathrm{IC}}^{\mathrm{app}}$, increasing its value without changing its evolution with d.

A toughening effect ($K_{\mathrm{IC}}^{\mathrm{app}} > K_{\mathrm{IC}}^{\mathrm{g}}$) is observed only for $V_{\mathrm{p}} > 5\,\%$, although for $V_{\mathrm{p}} = 10\,\%$ the apparent fracture toughness is not enhanced when $d > 16\,\mu$m. The maximum enhancement of $K_{\mathrm{IC}}^{\mathrm{app}}$ with respect to $K_{\mathrm{IC}}^{\mathrm{g}}$ is 1.3. Notice the toughening effect is generated by the improvement of mechanical properties

in the composite when increasing V_{p}, and not as a consequence of including residual stresses. This conclusion seems to be very difficult to observe through experiments. Moreover, in this case residual stresses never increase the apparent fracture toughness of the composite in this range.

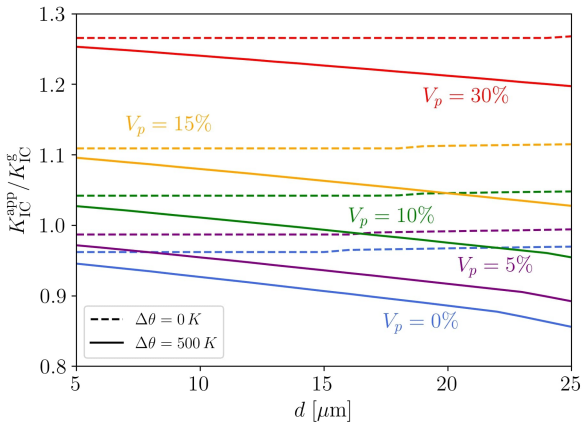

Figure 16: Effect of V_{p} on $K_{\mathrm{IC}}^{\mathrm{app}}$ at the scale of experiments for $\Delta\theta = 0\,K$ and $500\,K$ and $\alpha = 0°$.

The same analysis can be made considering an extended range of d, as it is shown in Fig. 17. An unpredictable effect of V_{p} is observed for large values of d. An increase of V_{p} generates a higher thermal expansion coefficient in the equivalent homogenized material, which reduces the compression residual stresses generated in the glass matrix during cooling, and consequently the negative thermal GSIF in the thermoelastic problem. As explained before, the negative GSIF led to an increase in $K_{\mathrm{IC}}^{\mathrm{app}}$, and it would be lower when increasing V_{p}. This effect is opposite to the one generated by the enhancement in the mechanical properties of the homogenized material when V_{p} is increased, that generally leads to a higher apparent fracture toughness. As a consequence, results are very difficult to estimate a priori when long platelets are considered, and residual stresses have a greater influence. A particular analysis is necessary to determine an optimal design of the composite in such region.

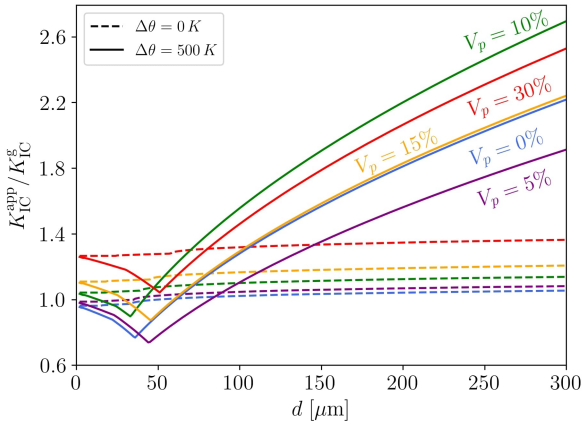

Figure 17: Effect of V_p on K_{IC}^{app} at the extended scale for $\Delta\theta = 0\,K$ and $500\,K$ and $\alpha = 0°$.

Furthermore, a toughening effect due to the presence of residual stresses is observed for long platelets, although this effect strongly depends on V_p. For such platelets, K_{IC}^{app} tends to increase, which means that it is the stress condition that is governing the failure. In particular, the value of K_{IC}^{app} is determined by the GSIF associated with the residual stresses, whose role is to close the crack (it is not possible to talk about positive or negative GSIFs here because they are complex in this case, see Section 5.1.2). Notice that the existence of a decreasing and increasing region in the evolution of K_{IC}^{app} allows us to determine a certain size of the platelet for which a minimum value of the apparent fracture toughness is obtained.

5.2.3. Comparison to experiments

Cannillo et al. [12] computed the residual stresses in the composite. Todd et al. [11] observed them experimentally and measured the tensile stress in the platelet through electron microscopy, expressing their results in terms of the mean stress $\bar{\sigma}_p = (\sigma_{11} + \sigma_{22})/2$, whereas the compressive residual stress in the matrix $\bar{\sigma}_m$ was calculated applying the equilibrium condition.

A comparison between these results [11, 12] and the ones obtained using the design tool presented in this work is made in Fig. 18. In order to obtain

the mean stress, a numerical simulation considering no mechanical loads and no pre-existing crack in the specimen was performed. It is important to highlight that in experiments several measurements were made at different points in the specimen, and that the only ones centered on the platelets were selected to carry out the comparison.

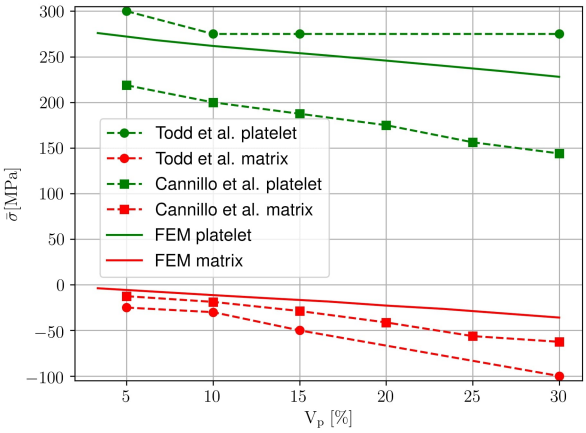

Figure 18: Residual stresses found in the literature [12] and [11] and residual stresses obtained in the simulations (FEM platelet and FEM matrix).

The difference between simulations made in this paper and experiments is greater for higher volume fractions. The reason could be that when a high concentration of alumina is considered, some clusters of platelets appear in the specimen [1], and therefore the theory of homogenization applied to calculate the mechanical properties of the composite in our model could differ from reality. The highest differences between experiments and numerical results are found in the platelet, where residual stresses calculated in this paper seem to be closer to experiments than the numerical data found in [12]. Moreover, using our design tool with one finite element calculation we are able to obtain the apparent fracture toughness for any platelet size, since the calculation is made in the inner domain (see Section 3). This strongly reduce the computational complexity of the analysis.

In Fig. 19 a validation of the model by comparison of the apparent fracture toughness with simulations is made. For each value of V_p two experimental measures of K_{Ic}^{app} are considered together with the mean value, see Table 2. The two extreme orientations of the platelet analyzed in this paper, $\alpha = 0°$ and $\alpha = 90°$ are used for the simulations, including the effect of residual stresses. A good agreement with experiments is observed for low values of V_p, since the average of the simulated values of K_{IC}^{app} between 0° and 90° falls within the error bar of experiments. For high values of V_p a greater difference is noticed, which can be explained by the clusters of platelets observed in the specimen for high concentrations of alumina, as it was mentioned above, that generate inhomogeneities in the material. Moreover, it is numerically and experimentally verified that the fracture toughness increases with the volume fraction of the composite in the material studied.

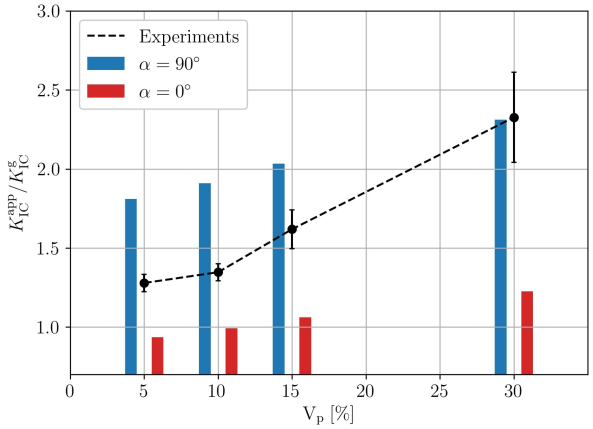

Figure 19: Comparison between experiments and simulations.

Throughout this paper, the effect of residual stresses in this kind of composites has been analyzed. Figs. 11b, 13b and 16 show that they do not have a strong effect in the fracture toughness at the experimental scale, considering several values of V_p and two possible orientations $\alpha = 0°$ and 90°. According to our numerical tool, the apparent fracture toughness estimated with residual

stresses is slightly greater than without residual stresses (about 10%). These conclusions were experimentally verified in [1], where K_{IC}^{app} is measured at room ($\Delta\theta \approx 500°$) and elevated temperature ($\Delta\theta \approx 0°$) for several values of V_{p}, showing that there is almost no difference between both cases (about 10%). In fact, they refer to this phenomenon as an apparent insensitivity of the toughening increment.

Another important study made in this paper is the path where the crack may be propagated. For $\alpha = 0°$, only a crack deflection is assumed, which is the one experimentally observed, but for $\alpha = 90°$ several options were analyzed. At the experimental scale and considering minor properties of alumina, it is concluded that penetration is the predominant mechanism among all the options (see Fig. 13b). This observation agrees with experiments in [8], which means that the alumina used seems to have low alumina fracture properties (although this information is unknown a priori). On the other hand, when major properties of alumina are used the predominant mechanism obtained according to our numerical tool is a lateral decohesion. This is in better agreement with numerical studies in [15] and [16].

6. Conclusions

A complete design tool for platelets composites is presented, particularized for the case of a glass matrix composite reinforced by alumina platelets. Two key novelties stand out from this methodology. First, it is a design tool in which multiple combinations are possible by modifying the input parameters of the composite, and therefore optimizing the design of platelets composites. Second, it offers the possibility to carry out a separate study of the different factors that are related to the fracture toughness: geometrical factors, such as the volume fraction, the size and the orientation of the platelet, or environmental factors, in particular the effect of residual stresses and the change in the pre-existing crack path. Furthermore, this design tool seems to have an important reduction in the computational complexity with respect to other analyses found in the

literature.

The following list summarizes the main conclusions obtained about the material studied throughout the paper:

- **Residual stresses:** It is not a general rule that they are a toughening mechanism. It depends on the size of the platelet and the change in temperature after cooling. The main parameter that explains why an enhancement of the apparent fracture toughness of the composite can be observed is the negative GSIF related to the thermoelastic problem (or its counterpart in the complex case). It is associated with a compression at the crack-tip, that must be overcome for crack propagation. Moreover, residual stresses promote lateral decohesion at the end of the platelet as a predominant failure mechanism in the composite. The effect of residual stresses is so high that the decohesion mechanism at the end of very long platelets can occur during cooling prior to any mechanical loading.

- **Size of the platelet:** when including the thermoelastic effect, longer platelets lead to a breakage after cooling down.

- **Volume fraction:** it has a positive scaling effect on the apparent fracture toughness of the composite. When the concentration of alumina is increased the deflection mechanism is promoted as a failure mechanism if alumina fracture properties are great enough, otherwise penetration is the governing mechanism.

The model proposed was studied at the scale of experiments found in the literature. First, the volume fraction has a bigger influence on the apparent fracture toughness than residual stresses, whose effect is very weak. Moreover, numerical results were verified by comparison with experimental results. The best agreement between them was found for low values of the volume fraction. This is because inhomogeneties were not considered in the analysis.

It is important to highlight that if the numerical tool is applied to a different material the conclusions obtained about the influence of residual stresses, the

size of the reinforcement, or the volume fraction might be different. Indeed, considering a very high volume fraction would lead to a completely different approach, even with the same constituents. One example is nacre-like ceramic made of alumina platelets (where $V_p \approx 90\%$), analyzed in [25, 26]. In that kind of materials the crack is propagated in a weak glass interphase between platelets.

Acknowledgments

The funding received from the European Union's Horizon 2020 research and innovation programme under Marie Skłodowska-Curie grant agreement No. 861061- NEWFRAC is gratefully acknowledged.

References

[1] M. Kotoul, J. Pokluda, P. Šandera, I. Dlouhỳ, Z. Chlup, A. Boccaccini, Toughening effects quantification in glass matrix composite reinforced by alumina platelets, Acta materialia 56 (12) (2008) 2908–2918. doi:https://doi.org/10.1016/j.actamat.2008.02.024.

[2] A. Winn, A. Boccaccini, N. Imam, P. Trusty, Examination of microhardness indentation-induced subsurface damage in alumina platelet reinforced borosilicate glass using confocal scanning laser microscopy, Journal of Microscopy 186 (1) (1997) 35–40.

[3] R. Joshi, R. Chhibber, Effect of sio2/b2o3 ratio on the thermophysical and wetting properties of borosilicate glass sealant for glass-metal joint, Journal of Materials Processing Technology 259 (2018) 186–194.

[4] K. Hu, S. Li, Z. Fan, H. Yan, X. Liang, Y. Cai, Q. Zhu, Y. Zhang, Contributions of mechanical bonding and chemical bonding to high-temperature

hermeticity of glass-to-metal compression seals, Materials & Design 202 (2021) 109579.

[5] S. R. Choi, N. P. Bansal, Mechanical properties of sofc seal glass composites, Advances in Solid Oxide Fuel Cells: Ceramic Engineering and Science Proceedings 26 (2005) 275–283.

[6] A. J. Thom, B. C. Tischendorf, L. B. Lohstreter, Advanced glass seals for implantable medical devices, Journal of the American Ceramic Society 105 (3) (2022) 1809–1820.

[7] Z. Liu, Y. Cai, K. Gong, C. Wang, Y. Zhang, Effects of al2o3 nanoparticles on the properties of glass matrix composites for sealant applications, Ceramics International.

[8] A. R. Boccaccini, P. A. Trusty, Toughening and strengthening of glass by al203 platelets, Journal of materials science letters 15 (1) (1996) 60–63. doi:https://doi.org/10.1007/BF01855614.

[9] A. Boccaccini, V. Winkler, Fracture surface roughness and toughness of al2o3-platelet reinforced glass matrix composites, Composites Part A: Applied Science and Manufacturing 33 (1) (2002) 125–131. doi:https://doi.org/10.1016/S1359-835X(01)00080-X.

[10] E. Bernardo, G. Scarinci, Sintering behaviour and mechanical properties of al2o3 platelet-reinforced glass matrix composites obtained by powder technology, Ceramics international 30 (5) (2004) 785–791. doi:http://dx.doi.org/10.1016/j.ceramint.2003.09.013.

[11] R. Todd, A. Boccaccini, R. Sinclair, R. Yallee, R. Young, Thermal residual stresses and their toughening effect in al2o3 platelet reinforced glass, Acta materialia 47 (11) (1999) 3233–3240. doi:https://doi.org/10.1016/S1359-6454(99)00177-9.

[12] V. Cannillo, C. Leonelli, A. R. Boccaccini, Numerical models for thermal residual stresses in al2o3 platelets/borosilicate glass matrix compos-

ites, Materials Science and Engineering: A 323 (1-2) (2002) 246–250. doi:https://doi.org/10.1016/S0921-5093(01)01345-4.

[13] C.-H. Hsueh, Sintering behaviour of powder compacts with multiheterogeneities, Journal of materials science 21 (6) (1986) 2067–2072.

[14] M. Taya, S. Hayashi, A. S. Kobayashi, H. Yoon, Toughening of a particulate-reinforced ceramic-matrix composite by thermal residual stress, Journal of the American Ceramic Society 73 (5) (1990) 1382–1391.

[15] V. Cannillo, G. Pellacani, C. Leonelli, A. Boccaccini, Numerical modelling of the fracture behaviour of a glass matrix composite reinforced with alumina platelets, Composites Part A: Applied Science and Manufacturing 34 (1) (2003) 43–51. doi:https://doi.org/10.1016/S1359-835X(02)00230-0.

[16] V. Cannillo, A. Corradi, C. Leonelli, A. Boccaccini, A simple approach for determining the in situ fracture toughness of ceramic platelets used in composite materials by numerical simulations, Journal of materials science letters 20 (20) (2001) 1889–1891. doi:https://doi.org/10.1023/A:1012870110675.

[17] S. Jiménez-Alfaro, D. Leguillon, Modelling of glass matrix composites by the coupled criterion and the matched asymptotics approach. the role of a single platelet, Theoretical and Applied Fracture Mechanics 122 (2022) 103650.

[18] P. Weißgraeber, D. Leguillon, W. Becker, A review of finite fracture mechanics: crack initiation at singular and non-singular stress raisers, Archive of Applied Mechanics 86 (1) (2016) 375–401.

[19] D. Leguillon, E. Sanchez-Palencia, Computation of singular solutions in elliptic problems and elasticity, John Wiley & Son, New York, 1987.

[20] W. Voigt, Ueber die beziehung zwischen den beiden elasticitätsconstanten isotroper körper, Annalen der physik 274 (12) (1889) 573–587. doi:https://doi.org/10.1002/andp.18892741206.

[21] D. Leguillon, Strength or toughness? a criterion for crack onset at a notch, European Journal of Mechanics - A/Solids 21 (1) (2002) 61–72. doi:https://doi.org/10.1016/S0997-7538(01)01184-6.

[22] D. Leguillon, E. Sanchez-Palencia, Fracture in heterogeneous materials, weak and strong singularities, in: P. Ladeveze, O. Zienkiewicz (Eds.), New Advances in Computational Structural Mechanics, Studies in applied mechanics, 32, Elsevier, Amsterdam, 1992, pp. 423–434.

[23] J. Rice, Elastic fracture mechanics concepts for interfacial cracksdoi:https://doi.org/10.1115/1.3173668.

[24] D. Leguillon, S. Murer, A criterion for crack kinking out of an interface, Key Engineering Materials 385 (2008) 9–12. doi:http://dx.doi.org/10.4028/www.scientific.net/KEM.385-387.9.

[25] A. Doitrand, R. Henry, J. Chevalier, S. Meille, Revisiting the strength of micron-scale ceramic platelets, Journal of the American Ceramic Society 103 (12) (2020) 6991–7000.

[26] T. Duminy, R. Henry, J. Adrien, A. Doitrand, S. Meille, Anisotropic fracture in nacre-like alumina, Theoretical and Applied Fracture Mechanics 123 (2023) 103710.